Green Chemistry

PAPER

View Article Online
View Journal | View Issue

Cite this: *Green Chem.*, 2022, **24**, 7458

Green chemical pathway of plasma synthesis of ammonia from nitrogen and water: a comparative kinetic study with a N_2/H_2 system†

Jungmi Hong, *‡[a] Tianqi Zhang, ‡[a] Renwu Zhou, *§¶[a] Liguang Dou, [b] Shuai Zhang, [b] Rusen Zhou,[a,d] Bryony Ashford, [c] Tao Shao, [b] Anthony B. Murphy, [c] Kostya (Ken) Ostrikov [d] and Patrick J. Cullen [a]

Sustainable ammonia synthesis under mild conditions that relies on renewable energy sources and feedstocks is globally sought to replace the current Haber–Bosch process. Electricity-driven plasma catalysis is receiving increasing attention as a sustainable technology for the efficient synthesis of ammonia. However, the current implementation of nonthermal plasma technology still faces several hurdles, particularly the extensive usage of energy-intensive H_2, low energy efficiency and the lack of understanding of the underlying mechanisms of the plasma catalysis process. Here we propose a green chemical pathway of plasma catalysis from nitrogen and water for sustainable ammonia production. In order to understand the different characteristics of the N_2/H_2O plasma system and seek further improvements in ammonia synthesis, detailed plasma kinetics modelling is presented in comparison with the N_2/H_2 system at atmospheric pressure. The model includes both electron and vibrational kinetics and updated surface reactions adapted from DFT calculation results on the SiO_2 surface. The facile dissociative adsorption of H_2O and the Eley–Rideal mechanisms are demonstrated to be important to enable efficient NH_3 production as the experimental observation. The model reproduced the measured trends of ammonia production on the different concentrations of H_2O input and power density with reasonable accuracy and provided an explanation of the critical influence of temperature and catalyst packing in the N_2/H_2O system in comparison to the N_2/H_2 system in relation to the quenching effect of H_2O by vibrational–translational relaxation.

Received 17th June 2022,
Accepted 1st September 2022

DOI: 10.1039/d2gc02299k

rsc.li/greenchem

Introduction

Artificial fixation of naturally abundant nitrogen (N_2) into human-required ammonia (NH_3) at a low cost is a key to sustaining the goal of carbon neutrality, as well as its dominant role in agriculture and potential competence in the hydrogen economy.[1,2] The well-established Haber–Bosch (H–B) process has already fed more than half of the global population for a century, but still suffers from meeting the demands for a green, decentralized, sustainable production of ammonia due to its endogenous conditions of harsh temperature and pressure (>150 bar; >450 °C) for driving the reaction forward.[3] The multi-million-dollar of capital investment prior to manufacturing also limits its decentralized production to support localized supplies, and the potential for developing essential infrastructure for remote areas and communities.[4] Among various strategies to complement and substitute the current H–B process, electrocatalysis and plasma-catalysis show promises to be integrated into renewable energy systems.[5,6] Nonthermal plasma systems have demonstrated efficient ammonia production under ambient conditions due to the highly reactive plasma species including high density electrons, ions, electronically and vibrationally excited molecules, atoms and radicals to circumvent significantly high energy requirements for dissociation of triple covalent N_2 bonds (bond energy

[a]*School of Chemical and Biomolecular Engineering, The University of Sydney, NSW 2006, Australia. E-mail: Jungmi.hong@sydney.edu.au, Renwu.Zhou@xjtu.edu.can*
[b]*Beijing International S&T Cooperation Base for Plasma Science and Energy Conversion, Institute of Electrical Engineering, Chinese Academy of Sciences, China*
[c]*CSIRO Manufacturing, Lindfield, NSW 2070, Australia*
[d]*School of Chemistry and Physics and QUT Centre for Materials Science, Queensland University of Technology (QUT), Brisbane, QLD 4000, Australia*
†Electronic supplementary information (ESI) available. See DOI: **https://doi.org/10.1039/d2gc02299k**
‡These authors contributed equally.
§Present address: State Key Laboratory of Electrical Insulation and Power Equipment, Centre for Plasma Biomedicine, School of Electrical Engineering, Xi'an Jiaotong University, Xi'an, Shanxi 710049, People's Republic of China.
¶This work was done while the author was working in University of Sydney.

946 kJ mol^{-1}). In particular, it is worthwhile to note the possible important role of vibrationally excited N_2 molecules with low threshold energy in plasma catalysis of ammonia to enable the energy efficient reaction pathway of ammonia production as reported by Mehta *et al.*[7] with its lowered activation energy barrier for dissociative adsorption and other related surface reactions.

Nevertheless, in general, the high energy consumption of plasma catalysis is noticed as where the most work needs to be done for improvement. As Sun *et al.*[5] demonstrated the significant improvement in energy efficiency by combining with the electrochemical process, this hybrid plasma and electrochemical process may provide a breakthrough to reach a satisfactory level of improvement both in energy consumption and production yield of ammonia. In addition, as in the successful example of NO_x production by Vervloessem *et al.* (2022) with a record-low energy consumption of 0.42 MJ (mol N)$^{-1}$, the application of pulse power may assist a significant reduction of energy requirement in ammonia synthesis as well by optimized vibrational–translational (V–T) non-equilibrium at a low reduced electric field E/N, which enhances the related chemical reaction but with minimized energy input.[8]

Apart from these few approaches to increase energy efficiency, seeking a different hydrogen source was our primary research aim to investigate an effective solution for green alternatives to the H–B process.

Various plasma types including microwave, radio frequency, arc, glow, and dielectric barrier discharge (DBD) have been used to provide improved production yield and energy efficiency of ammonia synthesis, in which most of the reports are based on the use of pure H_2 gas as a hydrogen source. Pure H_2 gas is produced predominantly by using fossil fuels, especially methane reforming but also from coal gasification with an enormous amount of CO_2 emission.[9,10] Hydrogen synthesis using electrolysis of water is possible and preferred from an environmental point of view. However, it requires significantly more energy and it is not considered to be feasible to compete with methane reforming at least for the next several decades.[11]

In addition, the hidden costs and environmental impact of the N_2/H_2 based ammonia process including purification, transport, storage, distribution, and safety consideration of highly combustible H_2 needs special attention.[12]

Therefore, substituting H_2 with H_2O as a hydrogen source for green NH_3 production is considered to be more environment-friendly, energy-saving, and industrially desirable.[13] A N_2/H_2O system, therefore, can clearly demonstrate its own benefits in comparison to the conventional approach based on a N_2/H_2 system. However, the production rate has been reported to be significantly low when it was compared to the result from N_2/H_2 plasma catalysis.[14–17]

Moreover, the detailed kinetic modelling of the N_2/H_2O plasma system including surface reactions has not been provided except for a brief suggestion on the possible pathway as described by Toth *et al.*.[16]

Recently, we have reported plasma-catalytic NH_3 synthesis based on a N_2/H_2O plasma system, achieving a NH_3 production rate of 65 μmol h^{-1} without a catalyst and 266 μmol h^{-1} when Ru/MgO was used.[18] The initial kinetic modelling work was reported mostly focused on Ru/MgO at a short time scale which has left a limitation to validate the measurement results and explain the different characteristics of ammonia synthesis in N_2/H_2O based plasma.[18]

In this study, the updated diffusion coefficient of gas species in a N_2/H_2O system and surface reaction data set based on DFT calculations have been implemented to explain ammonia synthesis in a concurrent reduction and oxidation environment in gas volume and on the surface. In addition, a new concept of dissociative adsorption of N_2 is introduced to be able to adapt the activation energy value from DFT calculation. The underlying mechanisms of NH_3 production in the N_2/H_2O system are analysed and compared with the N_2/H_2 system, and an efficient pathway to generate surface adsorbed $H_{(ad)}$ from a limited H_2O supply is demonstrated. The underpinning mechanism of the improved production rate and energy efficiency is discussed in relation to the critical importance of high gas temperature and catalyst packing in the N_2/H_2O system as an alternative process solution for the viable plasma synthesis of ammonia.

Plasma 0D kinetic modelling and DFT calculation

The zero-dimensional plasma kinetic solver ZDPlaskin[19] was used to perform plasma chemistry modelling in order to understand different mechanisms of ammonia production in a N_2/H_2O plasma system in comparison to the conventional N_2/H_2 system. The set of reaction equations related to N_2 and H_2O interactions written in the format as shown in eqn (1) is to be converted and merged into coupled differential equations with a component of production and loss reactions of individual species i as shown in eqn (2).[19]

$$aA + bB \rightarrow a'A + cC \quad (1)$$

$$\frac{d[N_i]}{dt} = \sum_{j=1}^{j_{max}} K_{ij}(t) \quad (2)$$

where $K_A = (a - a')K_j$, $K_B = -bK_j$, $K_c = cK_j$, $K_j = k_j[A]^a[B]^b$, N_i is the density of species i, and k_j is the reaction coefficient of reaction (1).

The coupled differential equation (eqn (2)) is solved combined with the Boltzmann equation solver BOLSIG+[20,21] providing the electron energy distribution and electron involved reaction rate such as attachment, excitation, ionization and a part of dissociation. In this model 77 gas and surface species are included with 1258 electron interactions, and gas phase and surface reactions as a summarized update from the previous N_2/H_2 model[22,23] in Table 1 and Tables S1, S2 in the ESI.†

Table 1 Gas phase and surface adsorbed species considered in the N_2/H_2O plasma model

Ground-state molecules and radicals	N_2, H_2O, H_2, O_2, O_3, NO, NO_2, NO_3, N_2O, NH_3, HNO, HNO_2, HNO_3, H_2O_2, HO_2, O_3, NH, NH_2, OH
Vibrationally excited molecules	$N_2(\nu_i, i = 1–8)$, $H_2O(\nu_i, i = 1–3)$, $H_2(\nu_i, i = 1–3)$
Electronically excited molecules	N_2(A3), N_2(B3), N_2(a′1), N_2(C3), H_2(B3), H_2(B1), H_2(C3), H_2(A3), H_2(R)
Atoms	N, N(2D), N(2P), H, O
Ions	N^+, N_2^+, N_3^+, N_4^+, H_2O^+, O^+, O_2^+, H^+, H_2^+, H_3^+, OH^+, NH^+, N_2H^+, NH_2^+, NH_3^+, NH_4^+, H^-, O^-, O_2^-, NH^+, N_2H^+, NH_2^+, NH_3^+, NH_4^+
Surface-adsorbed species	Surf, $H_{(ad)}$, $N_{(ad)}$, $O_{(ad)}$, $NH_{(ad)}$, $NH_{2(ad)}$, $NH_{3(ad)}$, $OH_{(ad)}$

Dissociative adsorption of H_2O and the further surface reactions related to water and oxygen are included and examined.

For this study, the diffusion coefficient D was recalculated using the first level of approximation by the Chapman–Enskog method for an approximate solution of the Boltzmann equation[24] in contrast to the same approximated diffusion coefficient applied for different gas phase nitrogen and hydrogen species in a previous N_2/H_2 model as 7.9×10^{-5} m^2 s^{-1} at 300 K and 1 atm. The collision integral data for interactions between N_2 and species containing nitrogen, hydrogen and oxygen are taken from Murphy (2012)[25] for N_2, H_2, N, H, NH_3 and NH, and Murphy (1995)[26] for NO, NO_2 and N_2O. The updated binary diffusion coefficient against a majority of N_2 molecules is provided based on this collision integral data in Table S3.† The temperature dependence on the calculated diffusion coefficient was considered proportional to $T^{3/2}$ for different gas temperature conditions in the model.

One of the most important improvements in our kinetic model is the description of dissociative adsorption. As noted in the introduction, there is a lack of understanding about the surface reaction under plasma catalysis with only a simplified interpretation of surface reaction probability. In particular, on a non-catalytic dielectric material, it is even worse often based on pure assumption.[23] Now with the availability of activation energy for the dissociation of nitrogen molecules from DFT calculation, the dissociative adsorption reaction is dealt as a two-step process: surface adsorption of molecules and the following event of dissociation on the surface as illustrated in Fig. 1. Accordingly, the reaction coefficient $k^*_{\text{diss.ads.}}$ is updated from eqn (3) to eqn (4) which is suggested as the product of the reaction coefficient of adsorption k_{ads}. and dissociation $k_{\text{L–H}}$ [27,28] as shown below.

$$k_{\text{diss.ads.}}[\text{cm}^{-6}\,\text{s}^{-1}] = \left[\frac{\Lambda^2}{D} + \frac{V}{A}\frac{2(2-\gamma_{\text{ads}})}{\bar{\nu}\gamma_{\text{ads}}}\right]^{-1} S_{\text{T}}{}^{-2} \quad (3)$$

$$k^*_{\text{diss.ads}}[\text{cm}^{-6}\,\text{s}^{-1}] = k_{\text{ads}} * k_{\text{L–H}} = \frac{\nu}{4}\left[\frac{\Lambda^2}{D} + \frac{V}{A}\frac{2(2-\gamma_{\text{ads}})}{\bar{\nu}\gamma_{\text{ads}}}\right]^{-1} \exp\left(\frac{-(E_{\text{d}}+E_{\text{a}})}{k_{\text{B}}T_{\text{w}}}\right) S_{\text{T}}{}^{-2} \quad (4)$$

Further DFT simulations have been performed to obtain the specific activation energy values for different steps of the

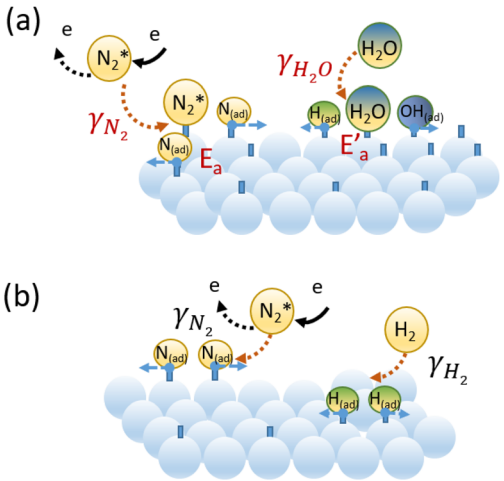

Fig. 1 (a) Illustration of the suggested two-step model for dissociative adsorption of N_2 and H_2O molecules and (b) previous model with representative sticking probability only where N_2* is for representing the higher contribution from the excited state of N_2 including vibrationally excited states $N_2(X,\nu_i)$.

hydrogenation reaction on the SiO_2 structure. The structural relaxation and electronic structure calculations were performed using the CASTEP module with the GGA and PBE functions in the Materials Studio package.[29,30] The exchange–correlation function is based on pseudo-potential-based plane-wave DFT and generalized gradient approximation as described by Perdew–Burke–Ernzerhof (GGA-PBE). The convergence criteria for energy, maximum force, stress, and energy cut-off were set at 2×10^{-5} eV per atom, 0.05 eV $Å^{-1}$, 0.1 GPa and 380 eV, respectively.

A density mixing electronic minimizer with a mixing scheme of Pulay was used and the convergence criteria for a self-consistent field (SCF) was set as 1.0×10^{-5} eV per atom. The Brillouin zone was sampled by a k point of $2 \times 2 \times 1$. Moreover, the transition states (TSs) are searched by means of the complete linear synchronous transit/quadratic synchronous transit (LST/QST) method for reactions,[31] and the convergence criterion for root-mean-square force on an atom is below 0.25 eV $Å^{-1}$.[32] To calculate the adsorption energy and energy barrier, a two-layer SiO_2(001) slab with a $p(2 \times 2)$ supercell containing 72 atoms was built and the impact of spin polarization was also considered due to the possible impact on the transition state of the reactions. The influence of spin polarization inclusion is discussed in detail in the ESI.† The atoms on the bottom two layers (36 atoms) are fixed in their optimized bulk coordinates, while the top two layers of the slab and the adsorbates are allowed to relax.

A vacuum of 12 Å along the Z-direction was applied to avoid interactions between periodic images. The adsorption energy (E_{ads}) is defined as follows:

$$E_{\text{ads}} = E_{\text{adsorbate/slab}} - E_{\text{adsorbate}} - E_{\text{slab}} \quad (5)$$

where $E_{\text{adsorbate/slab}}$ is the total energy of the slab together with the adsorbate, $E_{\text{adsorbate}}$ is the total energy of the isolated

adsorbate obtained in a 10 × 10 × 10 Å cubic cell, and E_{slab} is the total energy of the bare slab.

Experimental

The experimental results of NH_3 production from a N_2/H_2O system were taken from Zhang and Zhou *et al.*[18] using a single dielectric layer DBD configuration indicated as DBD-W. Here, as a comparison, NH_3 synthesis from a N_2/H_2 system was performed using the same reactor without catalyst packing under the same conditions, with a gas gap of 1 mm, applied peak voltage of 6.3(± 0.2) kV, and frequency of 33(± 0.3) kHz. The input H_2 gas concentration was set to 2.0 vol% to allow comparison with approximately 2 vol%. of H_2O used in the N_2/H_2O system.

The total flow rate was 1 L min^{-1}. The produced NH_3 was collected in water and the concentration was estimated using the Nessler's reagent method, as in Zhang and Zhou *et al.*[18] Five measurements were taken over 2 min and the average value was used for comparison with modelling results.

Results and discussion

Gas phase and surface adsorbed species in a N_2/H_2O system

In order to simulate a high flow rate (1 L min^{-1}), the plasma on time was limited to 0.06 s with approximately 1 cm^3 discharge volume. The reduced electric field of 82.3 Td was obtained from measurements as described in previous work.[18] The initial estimate of electron number density was 1.16 × 10^9 cm^{-3}, obtained using the QV Lissajous plot method as reported.[18] However, in order to match the same level of power density, a factor of 3.1 was multiplied and the modified value of 3.6 × 10^9 cm^{-3} was used as the spatially and temporally averaged electron density in the model for the nominal conditions of the empty reactor without a catalyst. This was justified by the good agreement between our previous N_2/H_2 model using averaged input parameters and van't Veer *et al.* which investigated the role of filamentary microdischarges and their afterglows.[33]

This is understandable considering the fact that ammonia is produced predominantly by surface reactions. The kinetic model showed the calculated density of NH_3 as 6.88 × 10^{14} cm^{-3} at 0.06 s as shown in Fig. 2(a), which corresponds to the production rate of 68.5 μmol h^{-1} which is close to the measurement of 65 μmol h^{-1} (ref. 18) of the production rate of NH_3 at the given plasma conditions.

In the experimental measurement, no NO_x was detected. Instead, N_2O was observed as the main N_xO_y product in our N_2/H_2O system at the given range of plasma conditions with significantly high number density than produced NH_3.[18] As in the experimental observation, NO_x species was calculated as in a low number density while the estimated number density of N_2O (4.6 × 10^{14} cm^{-3}, 46 μmol h^{-1}) showed a large gap from the measurements of over 570 μmol h^{-1}. Considering the fact

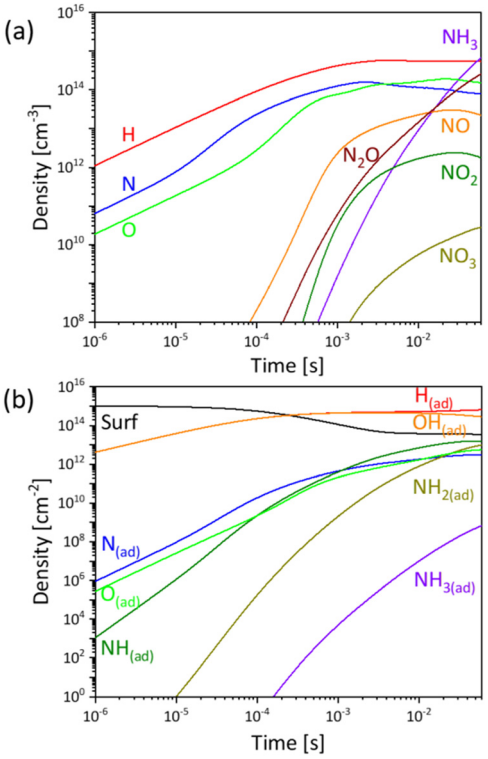

Fig. 2 Density profile of important species (a) in the gas phase and (b) on the surface where the residence time in plasma discharge is 0.06 s, constant E/N is 82.3 Td, n_e is 3.6 × 10^9 cm^{-3} and T_g is 500 K (assumed).

that N_2O was collected in the gas phase from a remote plasma area distant from the active discharge volume, a significantly high production rate of N_2O can be attributed to the recombination reaction between nitrogen, oxygen and NO_x species and/or a highly exothermic reaction between NH_3 and NO.[34] It is important to be aware of the possible environmental impact of N_2O as a highly effective greenhouse gas and ozone-depleting substance,[35,36] and hence it is necessary to examine its possible conversion or utilization in order to provide a more practical and viable green alternative to ammonia processing based on N_2/H_2O plasma.

Firstly, further oxidation of N_2O to convert into NO_x species in the subsidiary plasma module in an oxygen rich environment can be considered as a primary option as already suggested in our previous study.[18] More importantly, the interesting partial oxidation function of N_2O is worthwhile to note. Direct oxidation of benzene to phenol is a simple example of this type of reaction where the oxidation with O_2 cannot be accomplished by leading to the destruction of the aromatic ring and low phenol selectivity. In contrast, significantly high specificity of N_2O was found, and it is considered to be related to a particular state of anion radical oxygen species O^-_α (called α-oxygen), which forms on the a-sites from N_2O, but not possible from O_2.[37] Various different substrates includes alkanes, cycloalkanes, alkenes and aromatics have been investigated and the surface analysis results showed that the interaction with O^-_α in all tested cases enabled the selective formation of

hydroxylated products, revealing a remarkable potential of N_2O as a selective oxidant.[38,39] As recent important progress, it is reported that the insertion of N_2O into a Ni–C bond of the Ni catalyst enabled to deliver phenols with benign N_2 even at room temperature and 1.5–2 bar of N_2O conditions.[40]

N_2O has also been found to be equally important in homogeneous solution chemistry, including selective oxidation of highly reactive compounds such as disilenes or low-valent metallocenes and the synthesis of complex organometallic molecules as nitrogen donors.[41]

These potential revenues from N_2O and the possible high conversion rate of N_2O into NO_x seem to be positive evidence for continuing to develop this ammonia synthesis based on N_2/H_2O plasma to a further matured level of a green alternative and/or a complement process to the H–B process in the near future. A detailed discussion on the possible mechanism of N_2O production and loss in discharge volume and remote plasma region is provided in the ESI.† However, further investigation may require in order to validate these assumptions.

In addition to the density profile of the important gas species, as shown in Fig. 2(b), it is also important to note that in the N_2/H_2O plasma system, $H_{(ad)}$ and $OH_{(ad)}$ are the predominant species on the surface as it is considered to be generated mostly by dissociative adsorption of water. The details will be discussed in the following section.

Underlying mechanism of ammonia production in a N_2/H_2O system

In order to gain an insight into how this NH_3 production proceeds in a N_2/H_2O system, the important production and loss mechanisms were analysed using the graphical interface program QTPlaskin.[42] As shown in Fig. 3(a), NH_3 can be produced mostly by Eley–Rideal (E–R) interactions between the surface adsorbed $NH_{x(ad)}$ species and the hydrogen atoms and molecules which are predominantly generated by electron dissociation of H_2O and recombination of adsorbed $H_{(ad)}$ by gas phase H atoms.

For the loss mechanism of NH_3, the adsorption of the produced NH_3 back to the surface appears to be the predominant reaction. However, the facile desorption of NH_3 at a given wall temperature T_w of 473 K maintains the balance and supports the enhanced production of ammonia added to the major E–R interaction with hydrogen species. New loss channels of ammonia by atomic oxygen and OH radicals are found to be important next to the dissociation by electrons in the N_2/H_2O system.

The important intermediate species $NH_{(ad)}$ shown in Fig. 3(b) is mainly produced by E–R interactions between atomic nitrogen N and surface adsorbed hydrogen $H_{(ad)}$ or H atoms and $N_{(ad)}$ species on the surface. In this study, directly relevant activation energy values were introduced using DFT calculation for all hydrogenation steps of Langmuir–Hinshelwood (L–H) interaction and also dissociative adsorption of N_2 on the SiO_2 surface as shown in Fig. 4 and Table 2.

The DFT calculation result suggested that co-adsorption of $N_{(ad)}$ and $H_{(ad)}$ in the adjacent site is not available.

Hence, the L–H interaction between $H_{(ad)}$ and $N_{(ad)}$ is not available on the SiO_2 surface while the E–R interaction of gas phase hydrogen with surface adsorbed $N_{(ad)}$ is to be strongly preferred due to the strong electronegativity of the N atom. That means, once the N atom is bonded with the catalyst surface, the gaseous H atom can be easily captured by $N_{(ad)}$ rather than the neighbouring SiO_2 support. This new finding confirms the hypothesis on the important role of the E–R

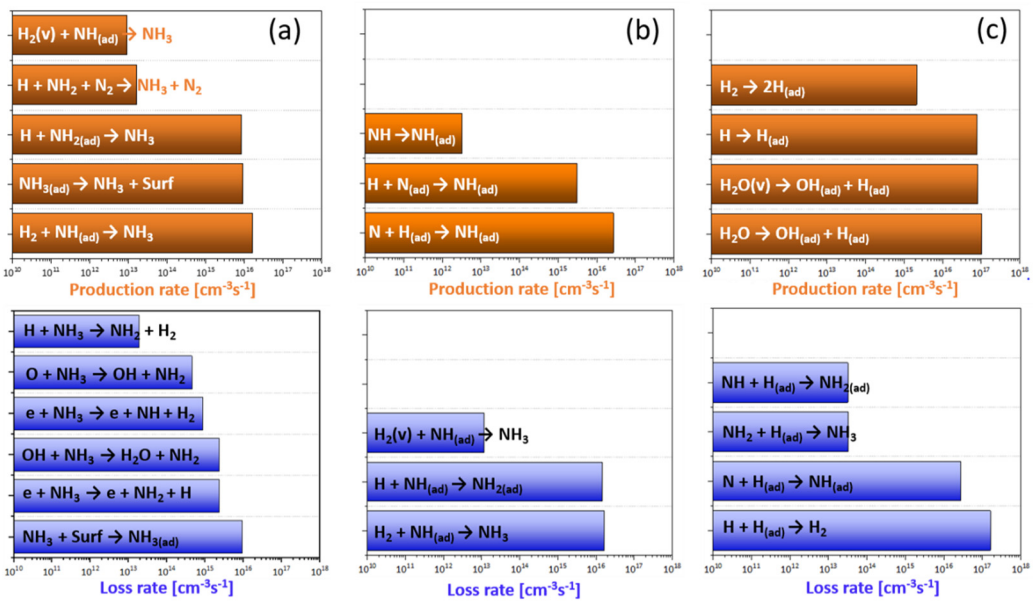

Fig. 3 Important reaction mechanism for the production and loss of (a) NH_3 (b) $NH_{(ad)}$ and (c) $H_{(ad)}$ where the residence time in plasma discharge is 0.06 s, E/N is 82.3 Td, n_e is 3.6×10^9 cm^{-3} and T_g is 500 K (assumed).

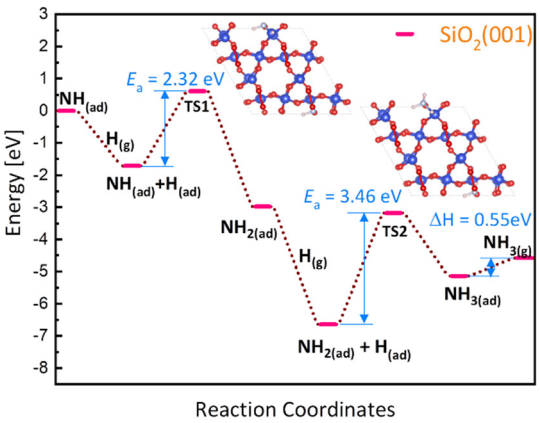

Fig. 4 DFT calculation result of the hydrogenation and dehydrogenation of $NH_{x(ad)}$ and desorption of $NH_{3(ad)}$.

Table 2 Summary of updated surface reactions from DFT calculations for the SiO_2 surface in comparison to Ru/MgO

	Activation energy E_a/desorption energy for NH_3	
Updated surface reactions	SiO_2	Ru/MgO
$N_2 + 2Surf \rightarrow 2N_{(ad)}$	7 eV (ref. 18)	1.07 eV (ref. 18)
$H_2O + 2Surf \rightarrow OH_{(ad)} + H_{(ad)}$	0.487 eV (ref. 43)	0.5 eV (ref. 44)
$N_{(ad)} + H_{(ad)} \rightarrow NH_{(ad)}$	N/A [this study]	0.96 eV (ref. 18)
$NH_{(ad)} + H_{(ad)} \rightarrow NH_{2(ad)}$	2.32 eV [this study]	1.67 eV (ref. 18)
$NH_{2(ad)} + H_{(ad)} \rightarrow NH_{3(ad)}$	3.46 eV [this study]	2.06 eV (ref. 18)
$NH_{3(ad)} \rightarrow NH_3$ (ΔH)	0.55 eV [this study]	0.9 eV (ref. 18)

interaction to proceed with further hydrogenation of $NH_{x(ad)}$ species in the N_2/H_2O system similar to N_2/H_2 plasma.[22,45,46] Not only do the H atoms have higher density in the discharge volume in comparison to nitrogen or oxygen atoms [Fig. 2(a)], but it is also worthwhile to note that the characteristics of fast thermal velocity and high diffusion coefficient of hydrogen [Table S3†] are one of the important contributing factors to enable higher surface reaction rates, such as for adsorption and the subsequent E–R mechanism, than those related to the N or O atom. These findings will be important to shed light on understanding the possible underlying mechanism of plasma synthesis of ammonia from nitrogen and water without the assistance of a catalyst where SiO_2 is one of the common reactor wall materials for various atmospheric pressure plasma applications.

The surface adsorbed $NH_{(ad)}$ forms $NH_{2(ad)}$ by interaction with gas-phase H atoms or directly produces NH_3 by reacting with ground-state and vibrationally excited H_2 molecules which is indicated as an important precursor to produce NH_3.

The use of H_2O was expected to interrupt the efficient reduction of nitrogen due to possible competing oxidation processes to produce N_xO_y and HNO_x species. However, the relatively low activation energy for the dissociation of water on SiO_2 resulted in preserving the high density of $H_{(ad)}$ on the surface which is an important precursor to initiate $NH_{(ad)}$ to proceed further with hydrogenation to complete NH_3 production in spite of limited supply of the hydrogen source.

The dissociative adsorption coefficients of molecules are calculated according to the newly suggested two-step model with a recently updated activation energy barrier E_a being higher than 7 eV (ref. 18) which suggests predominant $N_{(ad)}$ formation by atomic nitrogen on a non-catalytic SiO_2 surface. Fig. S4 and Table S7† show this correction in overestimated $N_{(ad)}$ by the N_2 molecule, particularly in the early stage and it resulted in a 1.2% decrease in NH_3 production in comparison to the conventional method of treating dissociative adsorption in the model while the rest of the gas and surface species remain the same.

Validation of the kinetic model with measurement results

In order to validate the model, a series of calculations has been performed as a function of electron densities or power densities and residence time within the discharge and H_2O content as shown in Fig. 5. To understand the influence of power and electron density on NH_3 synthesis, a different electron number density has been tested ranging from 1.2×10^9 to 4.5×10^9 cm^{-3} when the corresponding power density increases from 18 W cm^{-3} to 73 W cm^{-3}. Fig. 5(a) shows an overall increase in the number density of reactive gas phase species due to increased power and electron density. The number density of ammonia increased 4.5 times from 1.9×10^{14} cm^{-3} to 8.6×10^{14} cm^{-3} when the power density increased by a factor of 4. The increased density of atomic species of N, H and O and the radical NH and OH are expected since the main production mechanism of these atoms is by the electron interaction. NO_x and N_2O were also influenced by the increased electron density. Under oxygen 'deficient' conditions with a low water content, NO_x production appears to be limited to relatively low concentrations, with higher N_2O production instead.

As shown in Fig. 5(d), the measured maximum energy efficiency was 0.018 g kW h^{-1} at a specific energy input (SEI) of 1.33(± 0.15) kJ L^{-1} and decreased at higher SEIs up to 4 kJ L^{-1}. The average energy efficiency across the SEI range was 0.016 g kW h^{-1} with a small deviation (± 0.001 g kW h^{-1}), while the predicted value by the model showed a small increase as the SEI increases. This difference may be caused by the assumption of the constant reduced electric field E/N and electron density n_e input conditions adapted for our modelling work. As was reported in our previous study,[18] the measured current waveform includes very short time conduction current pulses. It may indicate that high density plasma with high instant electron density $n_e(t)$ is possible for that short time duration which can sustain high density reactive species to enable efficient ammonia production at low average power.

Fig. 5(b) shows the different production rates of each different gas species over residence time in the plasma discharge. Atomic species appears to be the predominant species at the early stage as expected and later smaller molecules such as NO shows a significantly increased production rate, followed by larger molecules such as NH_3 and N_2O.

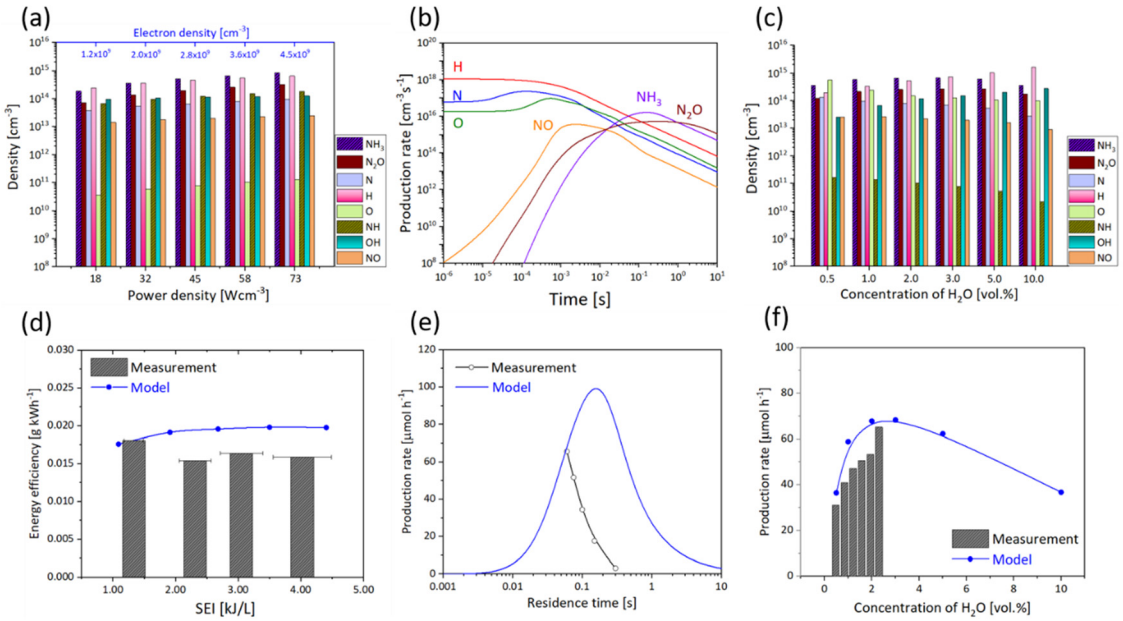

Fig. 5 Influence of electron density and power (a) and (b), residence time within the plasma (c) and (d) and concentration of H_2O (e) and (f) on ammonia production in N_2/H_2O plasma. (b), (d) and (f) shows the validation result with experimental data on the estimated ammonia concentration, where the E/N of 82.3 Td and T_g of 500 K were kept the same. H_2O, 2 vol% average; electron density n_e, 3.6 × 10^9 cm^{-3} and residence time, 0.06 s.

The experimental results indicated that changing the flow rate, and hence the residence time in the plasma, affected the production rate of ammonia.[18] The measured ammonia production rate was the highest at a maximum flow rate of 1 L min^{-1}. On the other hand, the model predicted that the maximum production rate occurs at around 0.16 s, which corresponds to a flow rate of approximately 0.4 L min^{-1} in Fig. 5(e). At high electron density and/or electron energy, the production rate profile curve can shift to the earlier time range. The fact that we have used the averaged electron density instead of a much higher instant electron density input can be the reason to shift the production rate profile to the longer residence time region in the model similar to what we have discussed on SEI dependence.

In the N_2/H_2O system, the amount of supplied H_2O is the most important governing factor. As the concentration of H_2O increases, Fig. 5(c) shows increasing H and OH as expected yet decreasing the atomic N and O number density.

The measurement results showed an increase in the production rate of NH_3 from 31 to 65 μmol h^{-1} as the saturated H_2O pressure increases from 5%(0.1 vol%) to 100%(2.3 vol%) at 300 K and the calculated result showed a good agreement from 36 to 68 μmol h^{-1} in Fig. 5(f).

At an input H_2O of 3 vol%, the estimated density of NH_3 showed a 1.5% increase in comparison to the nominal condition used in this model with 2 vol% H_2O input. Hypothetically, further increased H_2O content may provide more hydrogen sources, yet it can lead to significantly decreased ammonia density. It is possibly because of quenched vibrationally excited $N_2(\nu)$ molecules which result in a lowered energy gain of electrons and power density as well as reduced atomic nitrogen density as discussed in detail in section 6 in the ESI.†

Through the high rate of energy exchange with electrons and effective further excitation, dissociation and ionization, the role of vibrationally excited molecules is known to be significant in plasma discharges, especially under low-temperature atmospheric pressure plasma conditions.[47] It is also worthwhile to note the importance of $N_2(\nu)$[7,48] regarding the enhanced surface reaction rate for ammonia production and the discussion on the similar quenching effect of H_2O in CO_2 conversion application.[49–51]

The influence of H_2O through Vibrational–Translational (V–T) relaxation in the N_2/H_2O plasma system is confirmed in this study as shown in Fig. S5 and Tables S8, 9.† With and without V–T relaxation of $N_2(\nu)$ by H_2O considered, the vibrational distribution function of $N_2(\nu)$ shows significant differences. It is found that the addition of H_2O causes significantly decreased electron energy and overall reactive gas species density as well as an almost 3 times decrease in the production rate of ammonia at T_g 500 K mainly through V–T relaxation. It stresses the critical importance of V–T interaction in N_2/H_2O plasma and explains fundamental differences from ammonia production in the N_2/H_2 system regarding the influence on the electron energy and plasma density of the given system.

Comparison of ammonia synthesis with the N_2/H_2 system

Using the same DBD reactor, an ammonia synthesis experiment was performed with N_2/H_2 (0.98 : 0.02) at the same input power. The average production rate of NH_3 was 400(± 45) μmol h^{-1}, which is approximately 6 times that in the N_2/H_2O system.

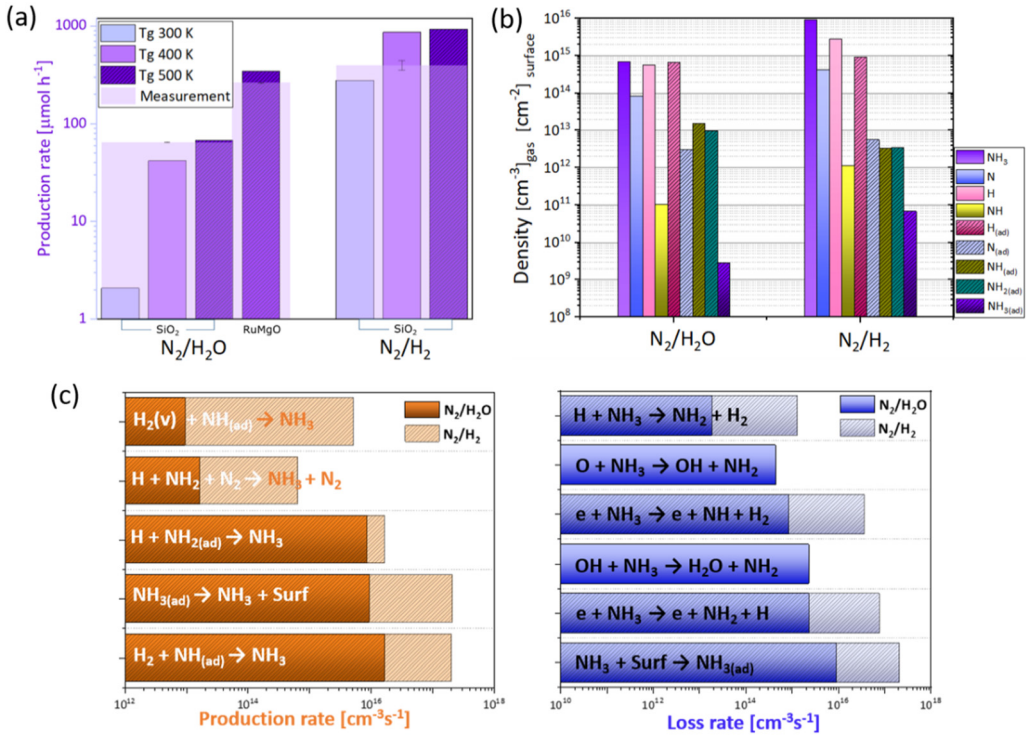

Fig. 6 Comparison of ammonia production in the N_2/H_2O and N_2/H_2 system: (a) production rate of NH_3 as a function of temperature with measurement results, where the gas temperature was assumed as the estimated rotational temperature based on N_2 molecular emission spectra in our previous study.[18] Considering the possible error, the measured production rate is presented in transparent pale pink across the whole temperature range for SiO_2 surface conditions, (b) important gas and surface adsorbed species and (c) production and loss mechanism where the *E*/*N* of 82.3 Td and T_g of 500 K were kept the same. H_2O, 2 vol% average; fixed power density, 58 (± 0.6) W cm^{-3}; residence time, 0.06 s except for Ru/MgO (*E*/*N*, 91 Td and power density, 70 W, based on the measurement results).

As shown in Fig. 6(a), the model predicted a 2.4 times higher production rate as 936 μmol h^{-1} for N_2/H_2 input conditions. Fig. 6(a) also includes the influence of gas temperature which is even more critical in the N_2/H_2O system than in the N_2/H_2 system.[45] This is considered to be because of the crucial impact of V–T relaxation of $N_2(\nu)$ by H_2O and its strong dependence on the gas temperature. Fig. S5† shows at a higher temperature of 500 K, the population of high-lying vibrationally excited states maintain a higher level in comparison to a lower temperature of 300 K due to the improved imbalance between excitation and de-excitation of $N_2(\nu)$ by H_2O. Therefore, in the plasma system including interactions with H_2O, the high gas temperature is favourable for maintaining the high density of high-lying $N_2(\nu)$ species, which then enables maintaining the high electron energy distribution and power density *via* efficient energy exchange of $N_2(\nu)$ with electrons.

In the N_2/H_2 system, the enhancement of ammonia production with increased temperature was attributed to improved NH_3 desorption and increased availability of active sites for nitrogen adsorption in order to realize the balanced surface reaction. However, in this updated N_2/H_2O model, particularly for non-catalytic silica-like surfaces, E–R interactions play a leading role, as we have discussed. Due to the negligible contribution from L–H interactions, even with highly saturated $H_{(ad)}$ and $OH_{(ad)}$ on the surface, the high reaction rate of the E–R mechanism enables a considerable amount of ammonia production similar to the measurement results.

In our previous work, it was demonstrated that by introducing an effective catalyst such as Ru/MgO it was possible to enhance the production rate of ammonia by a factor of 4 due to the high reactivity including a significantly low activation energy for the dissociation of N_2 of 1.07 eV.[18] As shown in Fig. 6(a), the modelling result with Ru/MgO surface properties supports the observation by generating 5 times increased ammonia number density under similar measurement conditions of 91 Td at 67.4 W cm^{-3}. It is important to stress that this significant increase by catalyst packing has not been reported in the N_2/H_2 system either in experimental or modelling results which often show increased production at best by approximately a factor of two in comparison to empty reactor conditions without a catalyst.[52,53] The characteristics of decreased electron energy distribution by V–T relaxation of $N_2(\nu)$ by H_2O explain the even further impact of reactive surface properties for efficient ammonia production in the N_2/H_2O plasma system. From the experiment, increased reduced electric field *E*/*N* and power density were observed by Ru/MgO catalyst packing as 91.0 Td, 68.5(± 3.5) W. With the same

plasma parameters, the calculated NH_3 density showed only a factor of 3 increase to 204 μmol h^{-1}. Therefore, the further increase is due to enhanced plasma properties which is a commonly observed augmentation effect in plasma catalysis.

As shown in Fig. 6(b), the N_2/H_2 system can produce higher densities of atomic N and H sustaining high electron energy without prohibiting the oxidation process in order to generate high density NH_3 molecules. With the same surface properties applied, in the N_2/H_2 system, the important production and loss mechanisms appear to be similar except for the loss mechanisms related to O and OH species. An increased E–R interaction between H_2 and $NH_{(ad)}$, particularly significant increase from vibrationally excited $H_2(\nu)$, is noticeable in the N_2/H_2 system.

It is possibly because apart from electron excitation, V–V′ interaction with $N_2(\nu)$ is one of the important excitation channels of $H_2(\nu)$.

Summary of the suggested mechanism of ammonia synthesis in the N_2/H_2O plasma system

As illustrated in Fig. 7, based on the results presented in earlier sections, the important reaction pathway can be summarized as follows:

1. Dissociation of N_2 and H_2O molecules by electrons

$$N_2 + e \rightarrow 2N + e, \quad H_2O + e \rightarrow H + OH + e$$

2. Direct surface adsorption

$$N + Surf \rightarrow N_{(ad)}, \quad H + Surf \rightarrow H_{(ad)}$$

$$NH_3 + Surf \rightarrow NH_{3(ad)}$$

3. Dissociative surface adsorption of H_2O

$$H_2O + 2Surf \rightarrow H_{(ad)} + OH_{(ad)}$$

4. E–R interaction to form the intermediate $NH_{x(ad)}$

$$N + H_{(ad)} \rightarrow NH_{(ad)}, \quad H + NH_{(ad)} \rightarrow NH_{2(ad)}$$

5. E–R interaction to produce NH_3

$$H_2 + NH_{(ad)} \rightarrow NH_3, \quad H + NH_{2(ad)} \rightarrow NH_3$$

6. Recombination by the E–R mechanism

$$H + OH_{(ad)} \rightarrow H_2O, \quad H + H_{(ad)} \rightarrow H_2$$

7. Desorption of surface adsorbed $NH_{3(ad)}$

$$NH_{3(ad)} \rightarrow NH_3 + Surf$$

8. Additional loss reaction of NH_3 from N_2/H_2

$$OH + NH_3 \rightarrow H_2O + NH_2, \quad O + NH_3 \rightarrow OH + NH_2$$

9. Oxidation reaction of nitrogen species

$$N_2{}^* + O_2 \rightarrow N_2O + O, \quad N^* + O_2 \rightarrow NO + O$$

where 'Surf' indicates the available empty active sites on the surface and the number of identified reactions is the same as in Fig. 7.

Electrons are crucial to provide dissociated atomic N and H species and initiate ammonia production, particularly with non-catalytic surfaces such as SiO_2 considered in this study. Direct adsorption of N and H is important to initiate further surface reactions. In contrast, gas-phase NH_3 also can be lost by surface adsorption. However, since this is balanced by efficient desorption at higher temperatures, it need not impact the whole process negatively. While the probability of $N_{(ad)}$ formation through dissociative adsorption is ruled out in this work, $H_{(ad)}$ is produced from the direct dissociation of water. Predominant E–R interactions explain the subsequent hydrogenation of $N_{(ad)}$ and the production of a NH_3 molecule under the surface conditions for which L–H interactions are limited. Surface-adsorbed species can leave the surface by the recombination process. Recombination of $OH_{(ad)}$ and $H_{(ad)}$ showed the highest reaction rate. As expected, in the N_2/H_2O system, additional dissociation pathways of NH_3 are possible by OH radicals or oxygen atoms in addition to the main loss mechanism by electrons as known from the N_2/H_2 kinetic model.[23,27,46]

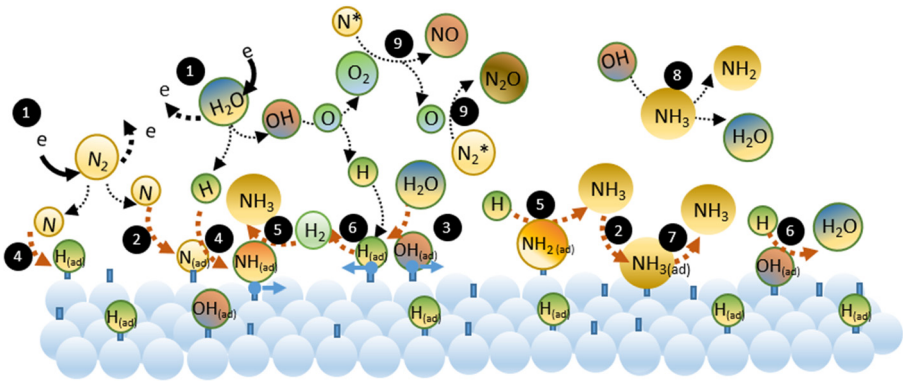

Fig. 7 Illustration of the suggested important pathway of ammonia production in N_2/H_2O.

Conclusions

Combined with DFT simulation, detailed chemical kinetic modelling of a N_2/H_2O atmospheric-pressure plasma system has been performed to assist in understanding the important mechanism of plasma catalytic production of ammonia from nitrogen and water. The treatment of the dissociative adsorption reactions has been improved by taking the calculated activation energy into account. The study has focused on SiO_2 surfaces, which are common reactor materials, in order to clearly elucidate the reactions, including in comparison to the N_2/H_2 system, without the complexity of the catalytic material.

As expected from the high activation energies, the model showed neither dissociative adsorption of N_2 nor stepwise L–H interactions of $N_{(ad)}$ or $NH_{x(ad)}$ which are chemical pathways for plasma synthesis of ammonia on non-catalytic surfaces.

A comparison of the predictions of the model with measurements showed differences in the input energy and the residence time dependence. A possible reason for treating the model with averaged constant plasma properties was discussed, which requires further consideration on applying time-dependent plasma parameters. However, the modelling results on the influence of power and H_2O concentration showed a good agreement, which suggests that this updated model of the N_2/H_2O system captures the important gas-phase and surface reactions.

Ammonia production is known to have a significant dependence on the surface reactivity, temperature and plasma conditions from different N_2/H_2 models. The same is also confirmed in the N_2/H_2O based system. However, the measurement[18] and the calculated modelling result suggest that it is even more crucial and has a far greater impact on N_2/H_2O plasma. Considering the important role of vibrationally excited $N_2(\nu)$ in exchanging energy with electrons and possibly enhanced chemical reactions including surface reactions, sustaining high gas temperature assisted with an optimized catalyst is suggested to be crucial to circumvent the inherent disadvantage of the quenching effect by H_2O molecules in the N_2/H_2O plasma system and maximize the production rate of ammonia at a reasonable energy cost.

Author contributions

J. H. and T. Z.: investigation, writing – original draft; R. Z.: methodology; L. D.: investigation; S. Z. and R. Z.: validation; B. A. and A. B. M.: writing – review & editing; T. S., K. O., and P. J. C.: conceptualization and supervision.

Conflicts of interest

There are no conflicts to declare.

Acknowledgements

This work was partially supported by the Australian Research Council (ARC) for Discovery Projects (grant number DP220102246) and the National Science Fund for Distinguished Young Scholars (grant number 51925703). We acknowledge the National Supercomputing Center in Shenzhen for providing the computational resources and the software.

References

1 A. Bogaerts, X. Tu, J. C. Whitehead, G. Centi, L. Lefferts, O. Guaitella, F. Azzolina-Jury, H.-H. Kim, A. B. Murphy, W. F. Schneider, T. Nozaki, J. C. Hicks, A. Rousseau, F. Thevenet, A. Khacef and M. Carreon, *J. Phys. D: Appl. Phys.*, 2020, **53**, 443001.

2 J. G. Chen, R. M. Crooks, L. C. Seefeldt, K. L. Bren, R. M. Bullock, M. Y. Darensbourg, P. L. Holland, B. Hoffman, M. J. Janik, A. K. Jones, M. G. Kanatzidis, P. King, K. M. Lancaster, S. V. Lymar, P. Pfromm, W. F. Schneider and R. R. Schrock, *Science*, 2018, **360**, 6391.

3 V. Kyriakou, I. Garagounis, A. Vourros, E. Vasileiou and M. Stoukides, *Joule*, 2020, **4**, 142–158.

4 D. Zhou, R. Zhou, R. Zhou, B. Liu, T. Zhang, Y. Xian, P. J. Cullen, X. Lu and K. Ostrikov, *Chem. Eng. J.*, 2021, **421**, 129544.

5 J. Sun, D. Alam, R. Daiyan, H. Masood, T. Zhang, R. Zhou, P. J. Cullen, E. C. Lovell, A. Jalili and R. Amal, *Energy Environ. Sci.*, 2021, **14**, 865–872.

6 K. H. R. Rouwenhorst, Y. Engelmann, K. van 't Veer, R. S. Postma, A. Bogaerts and L. Lefferts, *Green Chem.*, 2020, **22**, 6258–6287.

7 P. Mehta, P. Barboun, F. A. Herrera, J. Kim, P. Rumbach, D. B. Go, J. C. Hicks and W. F. Schneider, *Nat. Catal.*, 2018, **1**, 269–275.

8 E. Vervloessem, Y. Gorbanev, A. Nikiforov, N. De Geyter and A. Bogaerts, *Green Chem.*, 2022, **24**, 916–929.

9 World Energy Council, *World Energy Council, New Hydrogen Economy: Hope or Hype?*, 2019, **https://www.worldenergy.org/assets/downloads/WEInsights-Brief-New-Hydrogen-economy-Hype-or-Hope-ExecSum.pdf**.

10 R. W. Howarth and M. Z. Jacobson, *Energy Sci. Eng.*, 2021, **9**, 1676–1687.

11 S. Reed and J. Ewing, *Hydrogen is One Answer to Climate Change. Getting it is the Hard Part*, New York Times, 2021. **https://www.nytimes.com/2021/07/13/business/hydrogen-climate-change.html**.

12 A. Valera-Medina, F. Amer-Hatem, A. K. Azad, I. C. Dedoussi, M. de Joannon, R. X. Fernandes, P. Glarborg, H. Hashemi, X. He, S. Mashruk, J. McGowan, C. Mounaim-Rouselle, A. Ortiz-Prado, A. Ortiz-Valera, I. Rossetti, B. Shu, M. Yehia, H. Xiao and M. Costa, *Energy Fuels*, 2021, **35**, 6964–7029.

13 L. R. Winter and J. G. Chen, *Joule*, 2021, **5**, 300–315.

14 R. Hawtof, S. Ghosh, E. Guarr, C. Xu, R. M. Sankaran and J. N. Renner, *Sci. Adv.*, 2019, **5**, eaat5778.

15 Y. Gorbanev, E. Vervloessem, A. Nikiforov and A. Bogaerts, *ACS Sustainable Chem. Eng.*, 2020, **8**, 2996–3004.

16 J. R. Toth, N. H. Abuyazid, D. J. Lacks, J. N. Renner and R. M. Sankaran, *ACS Sustainable Chem. Eng.*, 2020, **8**, 14845–14854.
17 T. Haruyama, T. Namise, N. Shimoshimizu, S. Uemura, Y. Takatsuji, M. Hino, R. Yamasaki, T. Kamachi and M. Kohno, *Green Chem.*, 2016, **18**, 4536–4541.
18 T. Zhang, R. Zhou, S. Zhang, R. Zhou, J. Ding, F. Li, J. Hong, L. Dou, T. Shao, A. B. Murphy, K. Ostrikov and P. J. Cullen, *Energy Environ. Mater.*, 2021, 1–9.
19 S. Pancheshnyi, B. Eismann, G. J. M. Hagelaar and L. C. Pitchford, (**https://www.zdplaskin.laplace.univ-tlse.fr**), 2008.
20 BOLSIG+ computer code, **https://www.bolsig.laplace.univ-tlse.fr/**.
21 G. J. M. Hagelaar and L. C. Pitchford, *Plasma Sources Sci. Technol.*, 2005, **14**, 722–733.
22 J. Hong, S. Pancheshnyi, E. Tam, J. J. Lowke, S. Prawer and A. B. Murphy, *J. Phys. D: Appl. Phys.*, 2018, **51**, 109501.
23 J. Hong, S. Pancheshnyi, E. Tam, J. J. Lowke, S. Prawer and A. B. Murphy, *J. Phys. D: Appl. Phys.*, 2017, **50**, 154005.
24 A. B. Murphy, *J. Phys. D: Appl. Phys.*, 1996, **29**, 1922.
25 A. B. Murphy, *Chem. Phys.*, 2012, **398**, 64–72.
26 A. B. Murphy, *Plasma Chem. Plasma Process.*, 1995, **15**, 279.
27 E. Carrasco, M. Jimenez-Redondo, I. Tanarro and V. J. Herrero, *Phys. Chem. Chem. Phys.*, 2011, **13**, 19561–19572.
28 B. Gordiets, C. M. Ferreira, M. J. Pinheiro and A. Ricard, *Plasma Sources Sci. Technol.*, 1998, **7**, 363–378.
29 B. Delley, *J. Phys. Chem.*, 1996, **100**, 6107–6110.
30 M. C. Payne, M. P. Teter, D. C. Allan, T. A. Arias and J. D. Joannopoulos, *Rev. Mod. Phys.*, 1992, **64**, 1045–1097.
31 T. Halgren and W. Lipscomb, *Phys. Lett.*, 1977, **49**, 225–232.
32 Z. Han, Z. Yang and M. Han, *Appl. Surf. Sci.*, 2019, **480**, 243–255.
33 K. van 't Veer, Y. Engelmann, F. Reniers and A. Bogaerts, *J. Phys. Chem. C*, 2020, **124**, 22871–22883.
34 M. C. E. Groves and A. Sasonow, *J. Integr. Environ. Sci.*, 2010, **7**, 211–222.
35 M. Dameris, *Angew. Chem., Int. Ed.*, 2010, **49**, 489–491.
36 D. S. Reay, E. A. Davidson, K. A. Smith, P. Smith, J. M. Melillo, F. Dentener and P. J. Crutzen, *Nat. Clim. Change*, 2012, **2**, 410–416.
37 V. N. Parmon, G. I. Panov, A. Uriarte and A. S. Noskov, *Catal. Today*, 2005, **100**, 115–131.
38 P. P. Knops-Gerrits and W. J. Smith, in *Studies in Surface Science and Catalysis*, ed. A. Corma, F. V. Melo, S. Mendioroz and J. L. G. Fierro, Elsevier, 2000, vol. 130, pp. 3531–3536.
39 M. A. Rodkin, V. I. Sobolev, K. A. Dubkov, N. H. Watkins and G. I. Panov, in *Studies in Surface Science and Catalysis*, ed. A. Corma, F. V. Melo, S. Mendioroz and J. L. G. Fierro, Elsevier, 2000, vol. 130, pp. 875–880.
40 F. Le Vaillant, A. M. Calbet, S. González-Pelayo, E. J. Reijerse, S. Ni, J. Busch and J. Cornella, *Nature*, 2022, **604**, 677–683.
41 K. Severin, *Chem. Soc. Rev.*, 2015, **44**, 6375–6386.
42 QtPlaskin TRAPPA Group, **https://github.com/aluque/qtplaskin**.
43 J. Narayanasamy and J. D. Kubicki, *J. Phys. Chem. B*, 2005, **109**, 21796–21807.
44 A. Michaelides, A. Alavi and D. A. King, *J. Am. Chem. Soc.*, 2003, **125**, 2746–2755.
45 J. Hong, S. Prawer and A. B. Murphy, *ACS Sustainable Chem. Eng.*, 2017, **6**, 15–31.
46 J. Shah, W. Wang, A. Bogaerts and M. L. Carreon, *ACS Appl. Energy Mater.*, 2018, **1**, 4824–4839.
47 C. M. F. M. Capitelli, B. F. Gordiets and A. I. Osipov, *Plasma Kinetics in Atmospheric Gases*, Springer Berlin, Heidelberg, 2000.
48 K. H. R. Rouwenhorst, H.-H. Kim and L. Lefferts, *ACS Sustainable Chem. Eng.*, 2019, **7**, 17515–17522.
49 R. Snoeckx, A. Ozkan, F. Reniers and A. Bogaerts, *ChemSusChem*, 2017, **10**, 409–424.
50 T. Nunnally, K. Gutsol, A. Rabinovich, A. Fridman, A. Gutsol and A. Kemoun, *J. Phys. D: Appl. Phys.*, 2011, **44**, 274009.
51 A. Indarto, D. R. Yang, J. W. Choi, H. Lee and H. K. Song, *J. Hazard. Mater.*, 2007, **146**, 309–315.
52 J. Hong, M. Aramesh, O. Shimoni, D. H. Seo, S. Yick, A. Greig, C. Charles, S. Prawer and A. B. Murphy, *Plasma Chem. Plasma Process.*, 2016, **36**, 917–940.
53 Y. Wang, M. Craven, X. Yu, J. Ding, P. Bryant, J. Huang and X. Tu, *ACS Catal.*, 2019, **9**, 10780–10793.